Capability of Surface-Based Clear-Air Doppler Radar for Monitoring Meteorological Structure of Elevated Layers[1]

EARL E. GOSSARD

CIRES, University of Colorado, Boulder, CO 80309

RUSSELL B. CHADWICK, THOMAS R. DETMAN AND JOHN GAYNOR

NOAA/ERL/Wave Propagation Laboratory, Boulder, CO 80303

(Manuscript received 14 June 1983, in final form 1 November 1983)

ABSTRACT

Radars and acoustic sounding systems sense properties of the turbulence structure of the atmosphere. If atmospheric turbulence can be related to the mean gradient parameters, Doppler radars and acoustic sounders can provide information about height profiles of quantities such as temperature and refractive index as well as wind in stable regions of the atmosphere. In this paper turbulent and mean quantities were measured on the 300 m meteorological tower at the Boulder Atmospheric Observatory near Erie, Colorado, and the relationships between the turbulent and mean gradient quantities were examined in order to evaluate hypotheses for simplifying the kinetic energy balance and refractive index variance equations. FM-CW radar measurements of backscattered power and Doppler spectral width were also made for comparison with tower-measured refractive index spectra and Doppler velocity spectra. Height distributions of the turbulent dissipation rate within stable layers are shown and viscous cutoff radar wavelengths calculated.

1. Introduction

It is now well established that ground-based radars can sense the presence of many elevated meteorological layers (see Fig. 1). Radar backscatter from the clear air is generally assumed to result from scattering from inhomogeneities in the radio refractive index created by turbulent fluctuations in temperature and humidity (e.g., see Gossard and Strauch, 1983). It is often called Bragg scatter—a term we shall adopt here to avoid confusion with various other concepts of coherent and incoherent return. The strength of such backscatter is proportional to the structure parameter C_n^2 of the radar refractive index and so can be deduced from the measured backscattered power. The size of inhomogeneity important for such scatter is half the wavelength of the radar—in our case the radar wavelength was 10 cm. Furthermore, using backscatter from the clear air, Doppler radars are able to measure wind profiles under virtually all weather conditions, and can in principle observe turbulent intensity versus height by use of the width of the Doppler velocity spectrum. Two of the three measurable quantities are parameters of the turbulence structure and it is of considerable interest to find whether these measurables can be used to provide information about the profiles of mean quantities such as refractive index.

It is the purpose of the present paper to compare *in situ* measurements on a tower with radar measurements to test whether radars can accurately measure 1) the structure parameter of refractive index, C_n^2 and 2) the turbulent dissipation rate ϵ. We also examine relationships between turbulent and mean gradient quantities measured on the tower.

Finally, relationships between turbulent and mean gradient quantities have been developed only for scales lying in the inertial subrange of turbulence. Under very stable conditions the turbulent intensity can become very small, and there is the possibility that the Kolmogoroff microscale of turbulence becomes so large that the Bragg scale, which backscatters the radar waves, lies within the range of scales suppressed by viscous dissipation. Then, of course, deductions from radar return will be wrong. Therefore this paper also examines the inner scale.

2. Experimental set-up

The measurements were made at the Boulder Atmospheric Observatory (BAO) located near Erie, Colorado (Kaimal and Gaynor, 1983). This facility has a 300 m tower (Fig. 2) instrumented at 8 levels (10, 22, 50, 100, 150, 200, 250 and 300 m) with fast response sensors (see Fig. 3), such as platinum wire thermometers, sonic anemometers and a Lyman-α humidiometer (only on the carriage) and with accurate, but slow response, sensors such as quartz thermometers, propeller-vane anemometers and dew point hygrom-

[1] Work on this paper was sponsored by the Naval Ocean Systems Center; contract monitor: J. H. Richter.

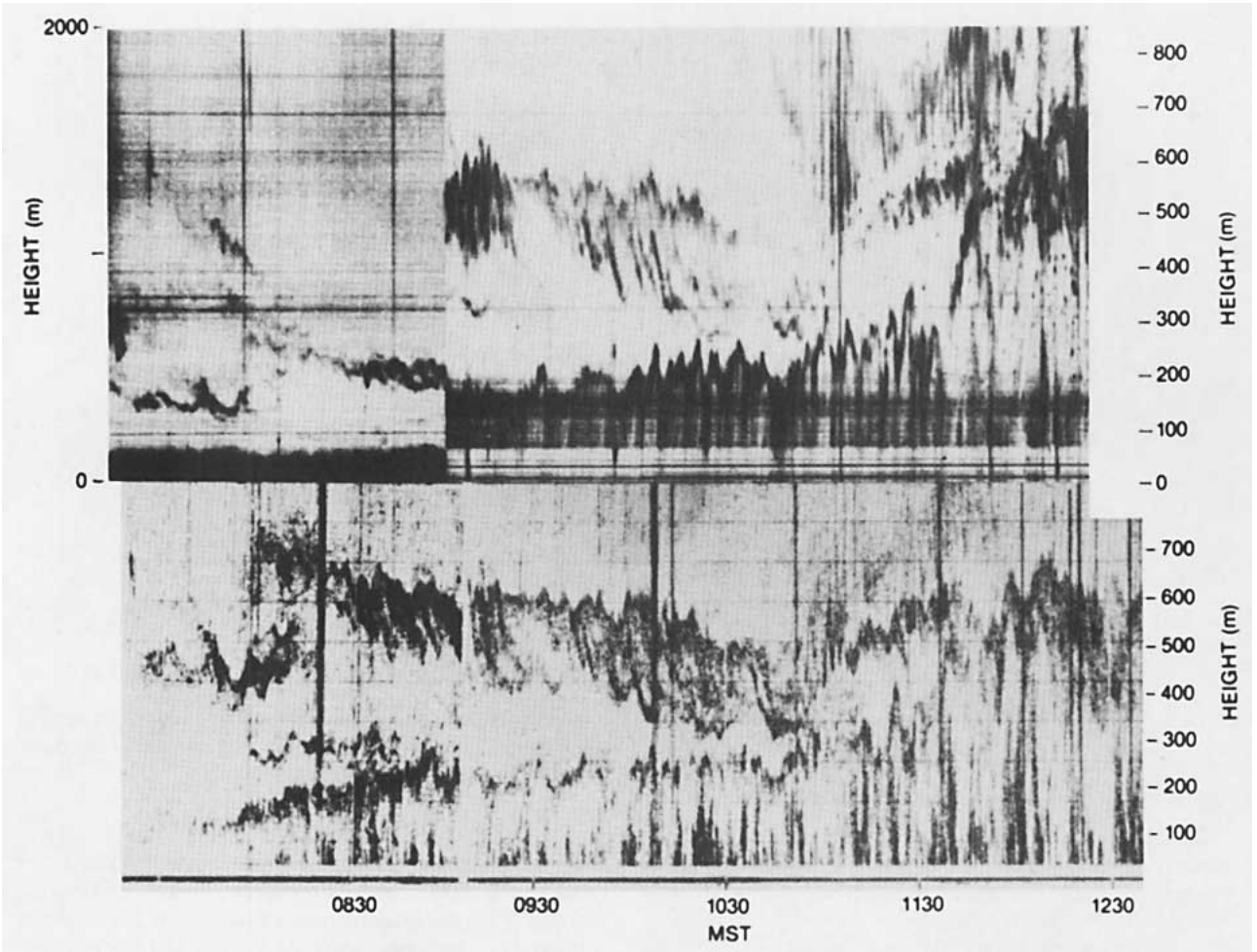

FIG. 1. FM-CW radar record (upper) and acoustic sounder record (lower) showing various surface and elevated layers. Height scale of radar record was changed to match acoustic sounder scale at 0845.

eters (Kaimal and Gaynor, 1983). These are distributed on the ends of two booms at each fixed level as shown in Fig. 3 and on a carriage that can be run up and down the tower configured as shown in Fig. 4. Thus, quantities such as C_T^2, C_q^2 and C_w^2 are obtained from the power spectra of time series recorded by the platinum wire, Lyman-α and sonic sensors, respectively and the gradient quantities are obtained from the quartz, dew point and propeller-vane sensors. As shown in Fig. 5 the carriage was placed midway between two fixed levels (150 and 200 m) at a height of 175 m. The gradients were obtained from measurements at the two fixed levels and the turbulent quantities were measured on the carriage boom midway between.

3. Relationship of radar refractive index spectrum to temperature and humidity spectra and to their cospectrum

The 300 m tower is not instrumented with a microwave refractometer, so radar refractive index must be calculated from temperature and the humidity "mixing ratio" provided by the Lyman-α humidiometer. In terms of mixing ratio (the ratio of water vapor density to dry air density),

$$N \equiv (n-1)\times 10^6 = \frac{77.6p}{T}\left(1+\frac{4.810q}{\zeta T}\right), \quad (1)$$

where n is radar refractive index; p is pressure in millibars; q is mixing ratio in grams per kilogram; T is temperature in kelvins (K); and $\zeta = 0.622$.

It is convenient to define a "potential refractive index" ϕ analogous to potential temperature so that we can work with a quantity conserved in adiabatic motion, which is a good assumption for the time and space scales characteristic of the turbulent inertial subrange. Referring (1) to a pressure level of 1000 mb and writing in terms of potential temperature θ, where $\theta = T(1000/p)^{0.286}$, and defining mixing ratio as grams per kilogram,

$$\phi = \frac{77600}{\theta}\left(1+\frac{7.73q}{\theta}\right). \quad (2)$$

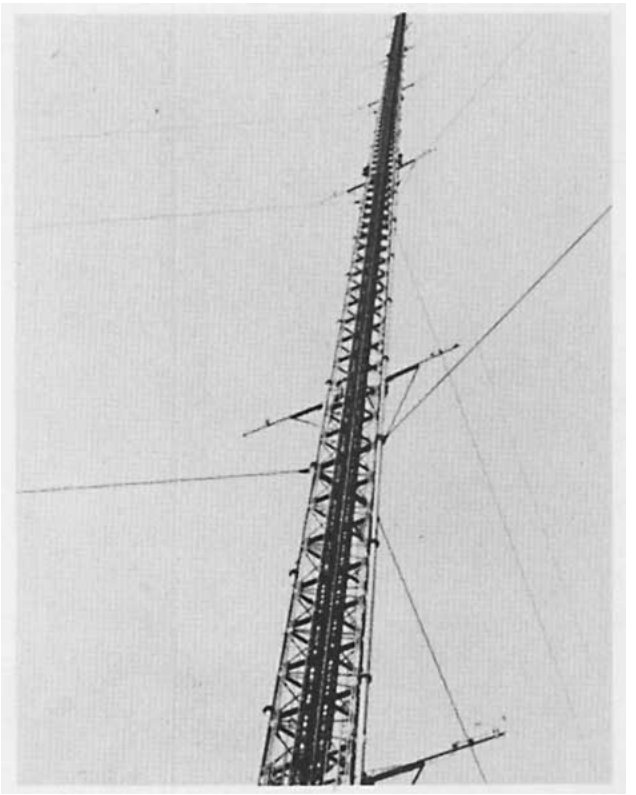

FIG. 2. The 300 m tower of the Boulder Atmospheric Observatory.

At any level the perturbations of ϕ and θ are small compared with the mean magnitude so, writing $\phi = \phi_0 + \phi'$, $\theta = \theta_0 + \theta'$ and $w = w_0 + w'$,

$$\phi' \approx -a\theta' + bq', \tag{3}$$

where for the data analyzed in this report,

$$a = \frac{77600}{\theta_0^2} + 1.2 \times 10^6 \frac{q_0}{\theta_0^3} \approx 1.04,$$

$$b = \frac{6.0 \times 10^5}{\theta_0^2} \approx 7.23.$$

Similarly, from (1),

$$N' = -a_N T' + b_N q', \tag{4}$$

where

$$a_N = \frac{77.6p}{\theta_0^2} + \frac{1200pq_0}{T_0^3} \approx 0.96,$$

$$b_N = \frac{600p}{T_0^2} \approx 6.68.$$

It follows that

$$\overline{\phi'^2} \approx a^2\overline{\theta'^2} + b^2\overline{q'^2} - 2ab\overline{q'\theta'}, \tag{5a}$$

$$\overline{N'^2} = a_N^2\overline{T'^2} + b_N^2\overline{q'^2} - 2a_Nb_N\overline{q'T'}, \tag{5b}$$

where

$$a^2 \approx 1.08, \quad b^2 \approx 51.8, \quad 2ab = 15.0$$

$$a_N^2 \approx 0.92, \quad b_N^2 \approx 44.9, \quad 2a_Nb_N = 12.9.$$

Furthermore, recalling that the power spectrum is the Fourier transform of the autocovariance function, (5a, b) show that (Gossard, 1960)

$$S_\phi \approx a^2S_\theta + b^2S_q - 2abS_{q\theta}, \tag{6}$$

where S_ϕ, S_θ and S_q are the power spectra of potential refractive index, potential temperature and mixing ratio, and $S_{q\theta}$ is the cross-spectrum (cospectrum) between temperature and humidity. If $S_{q\theta}$ has the same functional dependence on k as S_θ and S_q (i.e., $k^{-5/3}$ in the inertial subrange; see Wyngaard *et al.*, 1978),

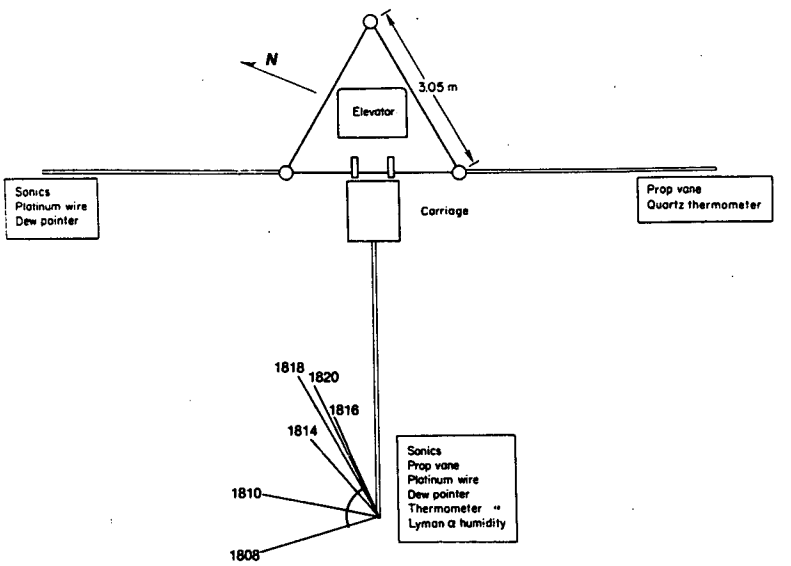

FIG. 3. Configuration of booms on the BAO tower and their instrumentation. "Dew pointer" stands for dewpoint hygrometer; "prop" stands for propeller.

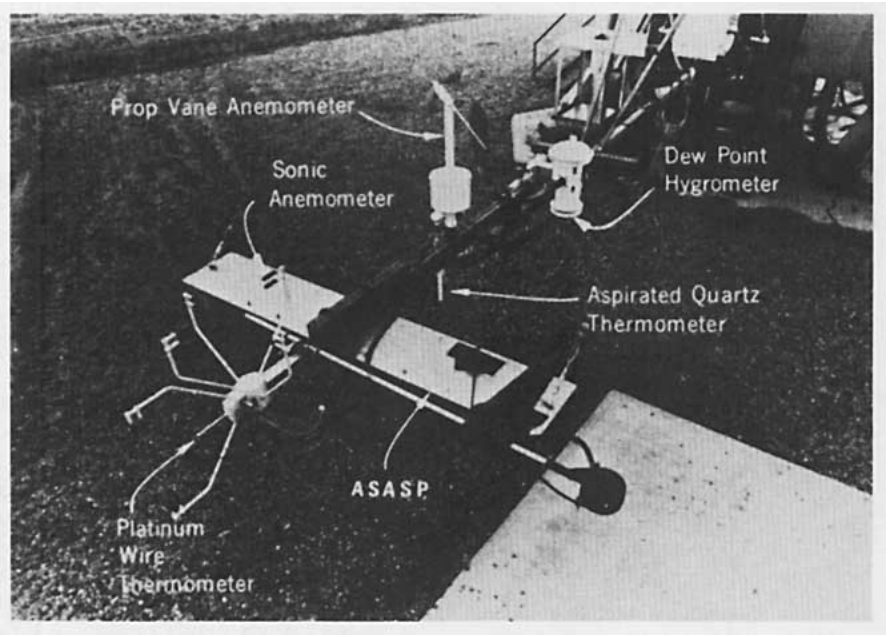

FIG. 4. Instrumentation on the carriage boom. Lyman-α humidiometer is not mounted in this photograph; Lyman-α is located 20 cm below platinum wire.

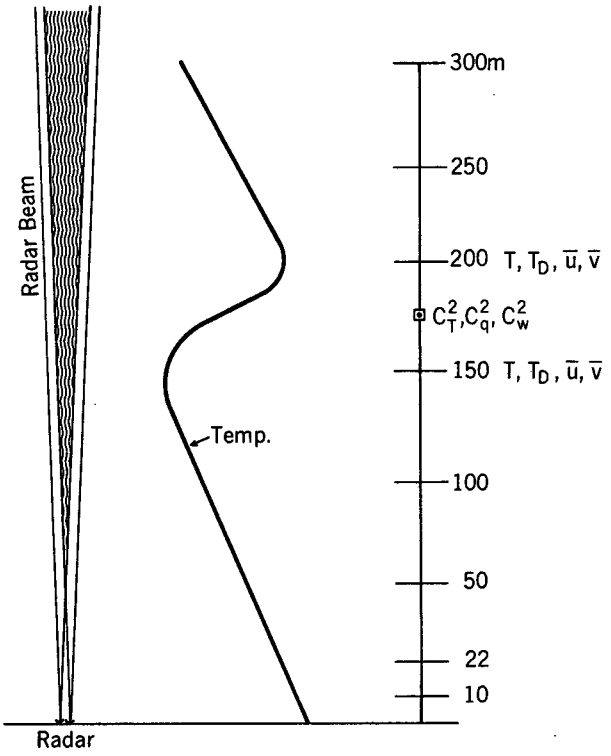

FIG. 5. Schematic configuration of tower/radar experiment. The radar was located about 550 m south of the tower. FM-CW radar beam shown schematically in left frame and tower in right frame. Schematic temperature profile with inversion lying across tower is shown in center. Accurate temperature (T), dewpoint (T_D) and horizontal wind ($\bar{u}$, $\bar{v}$) are measured at fixed levels. Carriage with turbulence sensors is placed midway between.

$$S_\phi = \frac{A_\phi}{B_\phi} C_\phi^2 k^{-5/3}, \tag{7}$$

where C_ϕ^2 is defined as in Table 1, and where A_ϕ and B_ϕ are the universal constants whose estimated values are given in Table 1. Therefore C_ϕ^2, C_θ^2, C_q^2 and $C_{q\theta}^2$ are related the same as the spectral quantities in Eq. (6) and values of C_N^2 and C_ϕ^2 were calculated from tower-measured values of S_T, S_q and S_{Tq} using Eq. (7). In the figures these values of C_N^2 have been called "measured". The power spectra of ϕ calculated from Eq. (6) are shown in Fig. 6 where the carriage measurements of S_q and S_θ were used to calculate S_ϕ. The importance of the cospectrum $S_{q\theta}$ is illustrated by Fig. 7 where the power spectra with and without the con-

TABLE 1. Turbulence parameters.

Velocity field	
$E(K) = \alpha\epsilon^{2/3}k^{-5/3}$,	$\alpha = 1.53$–1.68
$S(k_1) = A\epsilon^{2/3}k_1^{-5/3}$,	$A = 0.50$–0.55
$D_u(l) = \overline{[u(x+l) - u(x)]^2} = \underbrace{B\epsilon^{2/3}l^{2/3}}_{C_n^2 \text{ etc.}}$,	$B = 2.0$–2.2.
Refractive index field	
$E_\phi(k) = \alpha_\phi\epsilon^{-1/3}\epsilon_\phi k^{-5/3}$,	$\alpha_\phi = 1.33$–1.67
$S_\phi(k_1) = A_\phi\epsilon^{-1/3}\epsilon_\phi k_1^{-5/3}$,	$A_\phi = 0.8$–1.0
$D_\phi(l) = \underbrace{B_\phi\epsilon^{-1/3}\epsilon_\phi l^{2/3}}_{C_\phi^2}$,	$B_\phi = 3.2$–4.0.

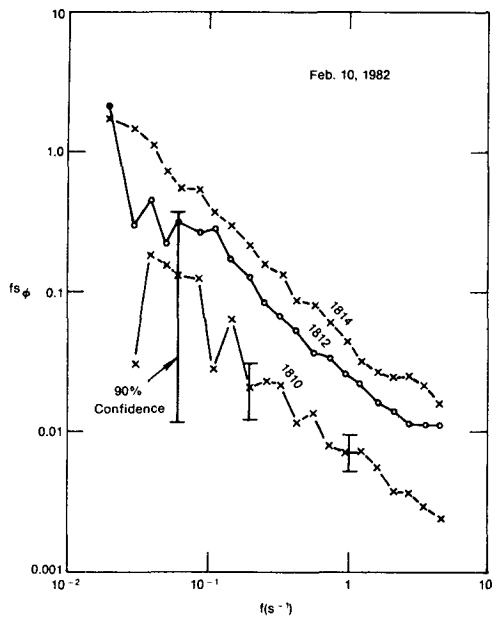

FIG. 6. Spectra of potential refractivity measured by platinum wire and Lyman-α humidiometer. Ordinate is power density times frequency.

tribution of the cross-power spectrum is shown along with the coherence between θ and q. Extrapolating out to a frequency of 37 Hz (which corresponds to the 5 cm turbulence length scale that is effective in the backscatter of 10 cm radar waves), we see that the cospectrum probably remains very important at the Bragg scale for our radar. The coherence was calculated from

$$\mathrm{Coh} = \left(\frac{\mathrm{Co}_{\theta q}^{\,2} + Q_{\theta q}^{\,2}}{S_q S_\theta}\right)^{1/2}, \tag{8}$$

where $\mathrm{Co}_{\theta q}$ and $Q_{\theta q}$ are the co- and quadrature spectra respectively. (Note that coherence must be essentially constant or negligibly small for Eq. (7) to be precisely true.)

4. Calculation of turbulence quantities from measured spectra

C_w^2 was obtained from the sonic anemometer spectrum of vertical velocity assuming Taylor's hypothesis to be a valid assumption to convert the temporal spectra to spatial spectra at the high wavenumbers of the inertial subrange. Typical spectra are shown in Fig. 8, where the values of $(^3/_4)C_w^{\,2} = C_u^{\,2} \equiv B\epsilon^{2/3}$ were evaluated at the frequencies indicated. The power in the inertial subrange, and therefore C_w^2, was arbitrarily evaluated at unity wavenumber corresponding to a frequency, f_0, found from the mean horizontal wind at that level;

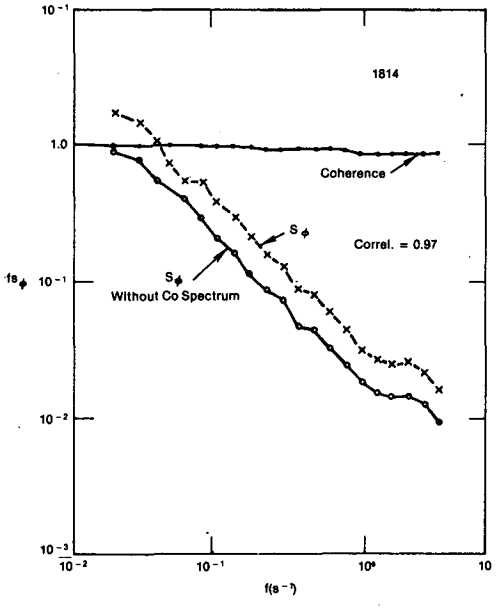

FIG. 7. Spectrum of potential refractivity with and without the contribution of cospectrum. Coherence between temperature and humidity. Lyman-α sensor located about 20 cm below platinum wire. Correlation between temperature and humidity is 0.97.

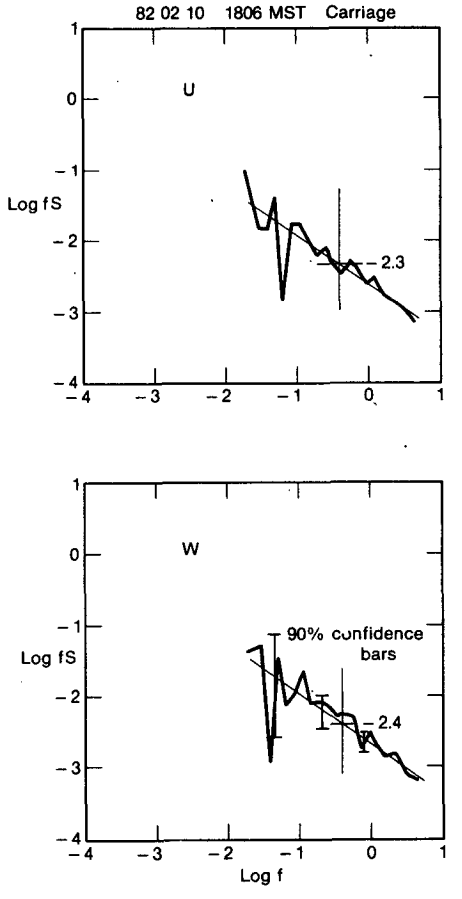

FIG. 8. Examples of velocity spectra with 90% confidence bars from sonic anemometers. Illustrates isotropy at large wavenumbers.

i.e., $f_0 = \bar{v}/2\pi$. Then, noting that $kS(k) = fS(f)$ where k is wave number,

$$C_w^2 = \frac{B}{A} f_0 S(f_0), \quad \epsilon = \left(\frac{f_0 S(f_0)}{A}\right)^{3/2}, \tag{9}$$

where ϵ is turbulent dissipation rate and B and A are $4/3$ of the values given in Table 1. After the calculation of f_0, the ordinate value $\log f_0 S(f_0)$ is simply read off of spectra such as Fig. 6, and C_w^2 and ϵ are calculated from (9). The ordinate values are read from lines with a slope of $-2/3$, drawn through each spectrum, which are a best fit to the high frequency (inertial subrange) portion of the spectrum. Note that a spectrum of form $f^{-5/3}$ yields a straight line with a $-2/3$ slope on a log log plot when $fS(f)$ is plotted against f. The temperature structure parameter C_T^2 was calculated as described for C_w^2 except the temperature spectrum was used instead of velocity, i.e.,

$$C_T^2 = \frac{B_T}{A_T} f_0 S_T(f_0), \quad \epsilon_T = \frac{f_0 S_T(f_0)}{A_T \epsilon^{-1/3}}, \tag{10}$$

where ϵ_T is rate of "dissipation" of temperature variance (actually half variance, or $\overline{T^2}/2$.

5. Relationships among turbulent quantities

As pointed out by Gossard *et. al.* (1982), there is a theoretical relationship among the height-gradient of mean refractive index in elevated stable layers, its structure parameter (calculable from the intensity of radar backscatter), vertical shear in the mean wind (measurable, e.g., by conical scans of a Doppler radar about a vertical axis), and the variance in the radial wind velocity [obtainable using the width (or 2nd moment) of the Doppler spectrum]. In this relation statistical steady state and negligible transport of variance have been assumed and the pressure terms in the turbulent kinetic energy budget equation have been assumed negligible in stable atmospheric zones. In deriving such relationships, Bragg backscatter is assumed in which the backscattered power is proportional to C_N^2 where $N = (n - 1) \times 10^6$ is called refractivity or modified refractive index and C_N^2 is its structure parameter; n, T, p and q are refractive index, temperature, pressure and humidity mixing ratio respectively. The analytical development is more conveniently done with "potential" refractive index ϕ, but N and C_N^2 are the quantities measured by *in situ* sensors and radars.

The results of Gossard *et. al.* (1982) are summarized by the relationships

$$C_\phi^2 = B_\phi \epsilon^{-1/3} K_\phi \left(\frac{\partial \phi}{\partial z}\right)^2,$$

where

$$\epsilon = \left(\frac{C_w^2}{B}\right)^{3/2}$$

and, if we assume $K_\theta = K_\phi$,

$$K_\phi = \frac{C_w^2}{\left|\frac{\partial \mathbf{v}}{\partial z}\right|^2 \left(\frac{K_m}{K_\theta} - \mathrm{Ri}\right) B^{3/2}},$$

whence

$$\frac{C_w^2}{C_\phi^2} \frac{\left(\frac{\partial \phi}{\partial z}\right)^2}{\left|\frac{\partial \mathbf{v}}{\partial z}\right|^2} = \frac{B}{B_\phi}\left(\frac{K_m}{K_\theta} - \mathrm{Ri}\right), \tag{11}$$

where ϕ is potential refractive index [see Eq. (1)], θ is potential temperature, $|\partial \mathbf{v}/\partial z|$ is gradient of the vector wind with height, $K_\theta = \overline{w'\theta'}(\partial\bar{\theta}/\partial z)^{-1}$, $K_m = \overline{w'u'}|\partial \mathbf{v}/\partial z|^{-1}$, Ri is the gradient Richardson number $[=(g/\bar{\theta})(\partial\bar{\theta}/\partial z)|\partial v/\partial z|^{-2}]$, B, B_ϕ are universal constants whose estimated ranges are given in Table 1, and C_w^2, C_ϕ^2 are structure parameters whose definitions are given in Table 1.

Overbars mean time average; for simplicity they have been left off of the height gradient quantities. These gradient quantities are typically obtained by averaging differences between fixed levels on the tower over two-minute intervals where each difference is a 10 s average of 10 Hz sampled data. The resulting averaged gradients were then used to calculate the Richardson number and various length scales. When the Richardson number was calculated from carriage traverses of the tower, it was found from each 10 s averaged data point.

The same reasoning that led to (11) leads to

$$\frac{C_w^2}{C_\theta^2} \frac{\left(\frac{\partial \theta}{\partial z}\right)^2}{\left|\frac{\partial \mathbf{v}}{\partial z}\right|^2} = \frac{B}{B_\theta}\left(\frac{K_m}{K_\theta} - \mathrm{Ri}\right) \tag{12}$$

for potential temperature, and a similar expression for humidity mixing ratio, q, whence

$$\frac{C_q^2\left(\frac{\partial \theta}{\partial z}\right)^2}{C_\theta^2\left(\frac{\partial q}{\partial z}\right)^2} = \frac{C_\phi^2\left(\frac{\partial \theta}{\partial z}\right)^2}{C_\theta^2\left(\frac{\partial \phi}{\partial z}\right)^2} = \frac{B_\phi}{B_\theta} = \frac{B_q}{B_\theta}. \tag{13}$$

There is no physical reason to suggest that B_ϕ/B_θ and B_q/B_θ are not unity, so (13) means that

$$C_q^2 \propto \left(\frac{\partial q}{\partial z}\right)^2, \quad C_\phi^2 \propto \left(\frac{\partial \phi}{\partial z}\right)^2 \quad \text{and} \quad C_\theta^2 \propto \left(\frac{\partial \theta}{\partial z}\right)^2$$

and that the proportionality constants are the same. This is just the reasonable statement that the power in the fluctuations is determined by the square of the gradient of the quantity for a given turbulent intensity, and that the turbulent intensity interacts with the mean gradients to create variance the same way for both θ and ϕ. However, length scales are defined by (see Tatarski, 1971, pg. 72)

$$\frac{C_q^2}{\left(\frac{\partial\theta}{\partial z}\right)^2} = L_q^{4/3} = \frac{C_\phi^2}{\left(\frac{\partial\phi}{\partial z}\right)^2} = L_\phi^{4/3},$$

$$\frac{C_\theta^2}{\left(\frac{\partial\theta}{\partial z}\right)^2} = L_\theta^{4/3}, \quad \frac{C_v^2}{\left|\frac{\partial\mathbf{v}}{\partial z}\right|^2} = L_v^{4/3} \tag{14}$$

so that (13) gives,

$$\left(\frac{L_q}{L_\theta}\right)^{4/3} = \left(\frac{L_\phi}{L_\theta}\right)^{4/3} = \frac{B_\phi}{B_\theta} = \frac{B_q}{B_\theta} = 1.$$

The length scales so defined are simply the vertical distance δ, through which a parcel must be mixed in a given gradient to cause a perturbation (variance) at its new level equal to the variance of the structure function for homogeneous, isotropic turbulence corresponding to a separation length equal to δ. Thus, it is a length scale, but it is more quantitatively defined than the classical Prandtl Mixing Length. Therefore (12) can be written

$$\frac{C_w^2}{C_\phi^2}\frac{\left(\frac{\partial\phi}{\partial z}\right)^2}{\left|\frac{\partial\mathbf{v}}{\partial z}\right|^2} = \left(\frac{L_v}{L_\phi}\right)^{4/3}. \tag{15}$$

The quantity $(K_m/K_\theta - \mathrm{Ri})$ that appears in (11) and (12) is virtually impossible to measure with accuracy because K_m and K_θ are so difficult to measure. This is because K_m and K_θ are defined in terms of covariance quantities that are mainly determined by the low frequency (small wavenumber) part of the spectrum; measurements are therefore very sensitive to long-term trends or gravity waves, although it is the contribution from the turbulence portion of the spectrum only that is wanted in the balance equations. Some kind of filtering must be done and almost any answer can be found depending on the filter used. In this paper, we propose to compare the various length scales and turbulence quantities of temperature, humidity and momentum, and we shall attempt to infer the magnitude and behavior of $(K_m/K_{\theta,\phi,q} - \mathrm{Ri})$ from measurements of C_T^2, C_v^2, C_q^2 and the mean gradients of temperature, wind and humidity. Note from (11) and (14) that the ratios of lengths to the $\frac{4}{3}$ power is the value of $(B/B_\theta)(K_m/K_\theta - \mathrm{Ri})$ inferred from (11).

In most cases directional shear in the mean wind is as important as speed shear, so it is shear of the vector wind that is important, and

$$\left|\frac{\partial\mathbf{v}}{\partial z}\right| = \left[\left(\frac{\partial u}{\partial z}\right)^2 + \left(\frac{\partial v}{\partial z}\right)^2\right]^{1/2}$$

is the important shear quantity where u and v are orthogonal components of the horizontal wind.

In addition to the length scales defined by (14), other classical turbulence lengths often discussed can be calculated from the data set with which we work here. These are:

The Outer Scale,

$$L_0 = 2\pi\left(\frac{2\alpha}{3}\right)^{-3/2}\overline{w'^2}^{3/2}\epsilon^{-1}, \tag{16}$$

where α is defined in Table 1.

The Buoyancy Scale,

$$L_B = \left(\frac{2}{c}\right)^{3/4}\pi\frac{\epsilon^{1/2}}{N^{3/2}}, \tag{17}$$

where

$$N^2 = \frac{g}{\bar{\theta}}\frac{\partial\theta}{\partial z}.$$

The Microscale,

$$\eta = \left(\frac{\nu^3}{\epsilon}\right)^{1/4}. \tag{18}$$

In the above, $\overline{w'^2}$ is the variance of vertical velocity, ν is kinematic viscosity and c is a constant assumed to be unity.

6. The case of 10 February 1982

In the climatic regime of Boulder strong elevated layers only rarely occur at tower levels where measurements of the kind described above can be made. On 10 February 1982, a relatively strong layer was recorded by the radar as it traversed the tower. The radar was operating unmanned, pointing vertically, and it cycled automatically between the Doppler mode and the backscattered-power-versus-range mode every minute; i.e., 15 s in Doppler and 45 s in range--power (see Fig. 9). Furthermore, at the time of this event the carriage was instrumented with the Lyman-α sensor and was stationary at the 175 m level. This coincidence is rare because the Lyman-α humidometer is only mounted on special occasions as it must be recalibrated frequently due to drift. Also, the raw 10 Hz data were being recorded at this time so that the spectra extend up to a frequency of 5 Hz (the Nyquist frequency). By contrast, the usual mode of operation only archives data averaged over a period of 10 s and "grab" samples of 10 Hz data taken every 10 s. For all of these reasons, this rare data set was analyzed intensively.

The time series of temperature and humidity are shown in Fig. 10 as the layer rose past the 175 m level, and the height profiles of temperature, wind and dewpoint between 1808 and 1814 are shown in Fig. 11. The height gradients used in calculating length scales during this time period were calculated from observations at the 150 m and 200 m levels bracketing the 175 m level where the turbulent measurements were made. The gradients were measured using the very accurate (but slow response) quartz thermometers and dewpoint hygrometers for temperature and humidity,

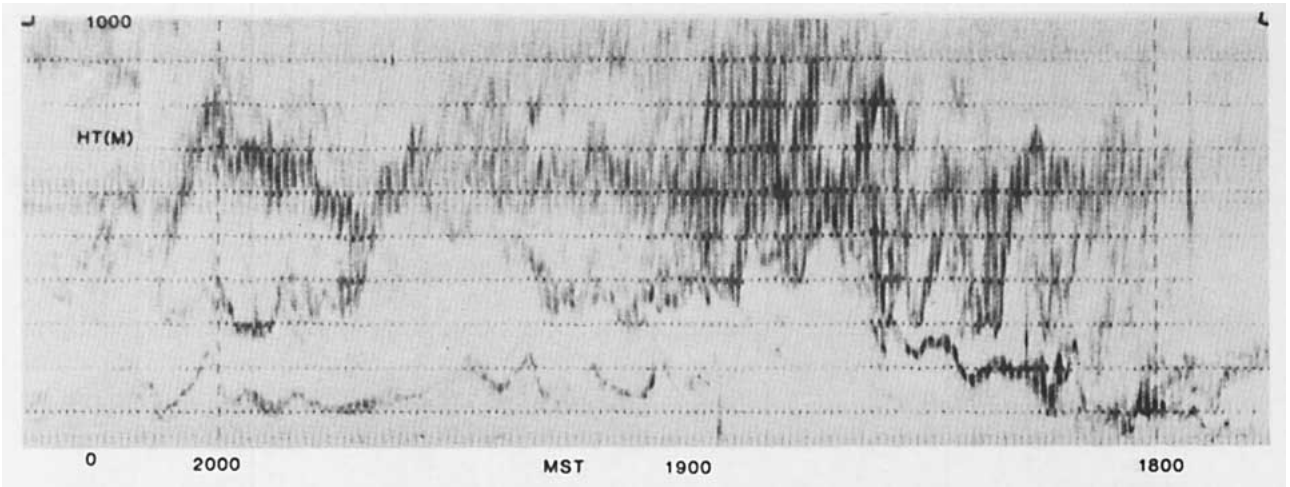

FIG. 9. The FM-CW radar record for 10 February 1982 showing wavy layer rising across the tower height range between 1800 and 1840. The radar measured backscattered power for 45 s then switched to the Doppler mode for 15 s producing the pattern of vertical strips. Vertical velocity in 9 range cells is indicated by the displacement of the quasi-horizontal lines of dots with 9 m s^{-1} in the separation between lines.

and the turbulence quantities were measured with the platinum wire thermometer, Lyman-α humidiometer and sonic anemometers on the carriage.

The observed and calculated values of the various turbulence quantities and length scales in the elevated layer are shown in Table 2. Fig. 12 shows calculated Richardson number and turbulent dissipation rate versus the ratios of length scales (and therefore inferred $(K_m/K_\theta - \mathrm{Ri})$ during the period. Unfortunately, a wind shift accompanied the event; so, as shown by the radial line segments representing wind direction in Fig. 3, the wind swung into a direction from the northeast that brought tower-generated mechanical turbulence to the carriage instruments after 1814. Therefore, it was necessary to use turbulence quantities from the 150 m and 200 m levels after 1814, and the averaged values for these levels are shown for 1816 and 1818 in Fig. 12. However large variations between levels

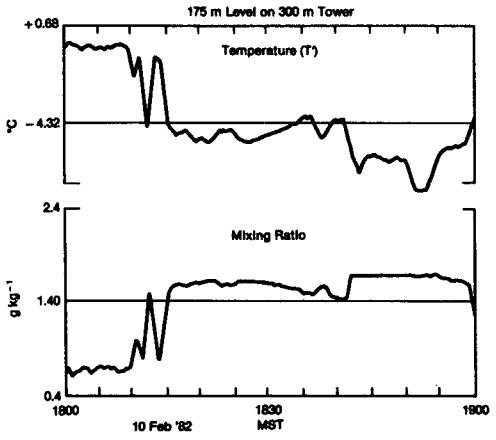

FIG. 10. Time series of temperature and humidity as the layer ascended upward past the carriage.

separated by 50 m were observed in the turbulence quantities so the 1816 and 1818 quantities are not considered to be very accurate. In Fig. 12 the agreement in the wavelength ratios for temperature and humidity is quite remarkable for the carriage turbulence values but, as is to be expected, the agreement is not so good with the averaged fixed-level values calculated for 1816 and 1818 when the wind had shifted through the tower. If the ratios of length scales are constant, (15) shows that any one of the four turbulent and gradient quantities on the lefthand side may be calculated if the other three can be measured. Ground-based Doppler radars can, in principle, measure the vertical wind shear, $|\partial v/\partial z|$, C_v^2 (from the Doppler spectral width) and C_n^2 (from the strength of the backscattered power). From these three measurables, the refractive index gradient aloft, $\partial\phi/\partial z$, can then be calculated. Fig. 12 suggests that $(B/B_\theta)(K_m/K_\theta - \mathrm{Ri})$ is approximately unity and there is no obvious dependence on either Ri or ϵ although this sample is, of course, very small.

Figure 13 shows the plot of C_T^2 and $C_n^2 = C_N^2 \times 10^{-12}$ at the carriage during the time interval when the echo layer rose past the 175 m level where the carriage was located. The C_N^2 were calculated from the platinum wire temperature spectra and the Lyman-α humidity spectra as described earlier. Fig. 14 shows the height profile of C_n^2 measured by the radar at 1814, and the agreement between the radar measurements and the *in situ* measurements at 175 m is very satisfactory.

7. Calculation of C_w^2 from Doppler spectral width

The following factors may cause broadening of the radar Doppler velocity spectrum (e.g., Gossard and Strauch, 1983):

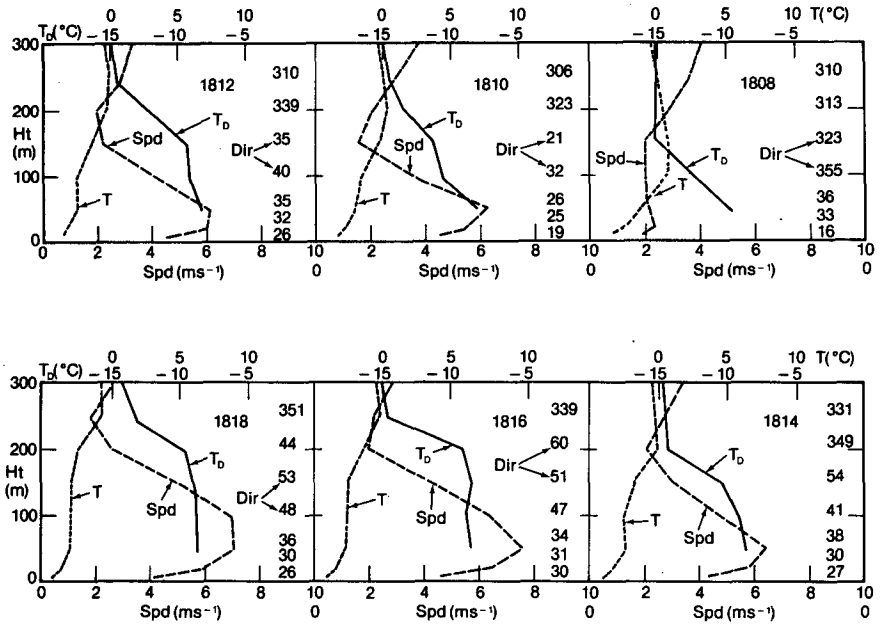

FIG. 11. Wind and temperature profiles across the tower at the times shown on 10 February 1982.

(a) If there is wind shear, the speed and direction of the mean wind may vary significantly within a range cell, causing spectral broadening. A velocity gradient transverse to the beam axis is usually more important than a radial velocity gradient. These can be very important effects for most radar configurations, but in the present experiment these effects are negligible because the radar antenna points vertically; thus any vertical shear in the horizontal wind is longitudinal to the beam axis and has no effect on the *radial* velocity component which in this case is vertical velocity and small to begin with.

(b) The Doppler spectrum is broadened if the antenna moves, but in the present experiment the antenna was stationary.

TABLE 2. Observed turbulence quantities and scales.

Time (MST)	1808	1810	1812	1814	1816*	1818
Ri	0.18	0.48	0.66	0.43	0.59	0.36
L_0 (m)	54.1	288.0	401.0	4.8	21.8	50.5
L_B (m)	69.0	47.6	93.3	58.8	43.1	90.0
L_θ (m)	32.8	8.1	9.9	11.4	2.1	4.2
L_v (m)	13.8	6.7	7.7	8.4	3.9	3.3
L_q (m)	32.4	8.1	9.9	11.3	1.8	2.5
L_ϕ (m)	46.7	5.8	10.6	11.1	1.9	4.7
ϵ (cm^2 s^{-3})	13.8	9.7	13.8	54.7	3.8	3.0
η (cm)	0.11	0.12	0.11	0.08	0.16	0.16
λ_c (cm)	2.8	3.1	2.8	2.0	2.8	2.8
Pr	0.72	1.8	1.9	1.6	1.85	1.5

* Wind to carriage passed through tower. Turbulence measurements averaged between booms at 150 m and 200 m levels relatively unreliable.

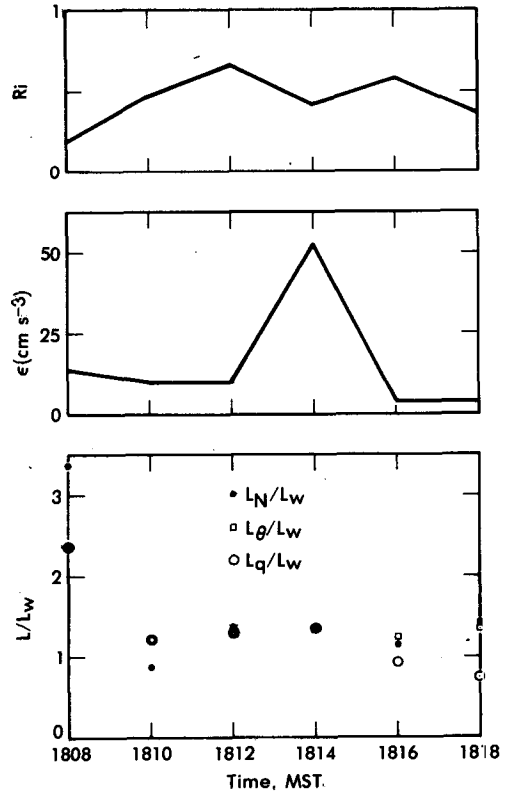

FIG. 12. Ratios of various length scales compared with Richardson number Ri and turbulent dissipation rate ϵ. At 1808 turbulent fluctuations in temperature were very small ($C_T^2 = 1.4 \times 10^{-3}$, see Fig. 13) and the temperature difference used to calculate $\partial\theta/\partial z$ was only 0.32, so the 1808 values must be considered to be of lesser accuracy than those of 1810–1814.

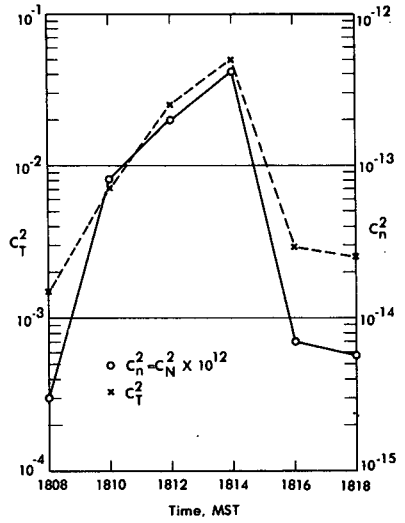

FIG. 13. Temporal variation of C_T^2 and C_n^2 as layer rises across sensors at 175 m.

(c) Even if there is no turbulence or shear in the mean wind, so that it is completely uniform in speed and direction, the Doppler spectrum would have finite width because of the width of the radar beam; that is, if the beamwidth is not infinitesimal, the radial direction from the radar varies over the beam so that a range of radial velocities is sensed even if the wind is uniform. However, in the present experiment the radar beamwidth is only 2.5 degrees so this effect is small.

(d) If all scattering centers within each radar range cell move with the same velocity, the Doppler spectral frequency will be merely shifted according to the component of velocity radial to the radar. However, if there is turbulent movement of the scattering centers within the range cell toward and away from the radar, the spectral line will be not only shifted but broadened according to the turbulent intensity.

Only the last factor (d) should be important for the configuration chosen in this experiment (see Fig. 5), and this factor will now be discussed.

If x is the direction of propagation, Gaussian antenna patterns in both angle and pulse length are proportional to $\exp[-(k_x^2b^2 + k_y^2a^2 + k_z^2a^2)]$, where a and b are the (Gaussian) beamwidth and range cell length, respectively. Then (Frisch and Clifford, 1974, with corrections pointed out by Labitt, 1981),

$$\epsilon = \delta^{-1}\{\sigma_{11}^2[1.35\alpha(1 - \gamma^2/15)]^{-1}\}^{3/2} \qquad (19)$$

to 2nd order of a hypergeometric series expansion, where

$$\delta = a, \quad \gamma^2 = 1 - (b/a)^2 \qquad \text{for} \quad b/a < 1,$$

$$\delta = b, \quad \gamma^2 = 4[1 - (a//b)^2] \quad \text{for} \quad a/b < 1,$$

and σ_{11}^2 is the velocity variance in the radial (say x) direction. For isotropic turbulence, in the inertial subrange,

$$C_u^2 = \left(\frac{3}{4}\right)C_v^2 = \left(\frac{3}{4}\right)C_w^2 = B\epsilon^{2/3}, \qquad (20)$$

so

$$C_w^2 = \left(\frac{4}{3}\right)B\delta^{-2/3}\sigma_{11}^2[1.35\alpha(1 - \gamma^2/15)]^{-1}, \qquad (21)$$

where

$$\sigma_{11}^2 = \frac{\int (v_{11} - \bar{v})^2 S(v)dv}{\int S(v)dv}$$

and $S(v)$ is the velocity spectrum observed by the Doppler radar.

Values of ϵ measured at the 175 m level on the tower are compared with radar-measured values at a height of 200 m (with 100 m resolution) in Fig. 15. These are easily converted to C_w^2 using Eq. (20). Considering the 550 m separation of the radar and the tower these results are in fair agreement. However, in general they do not agree well even when the volume averaging by the radar and the time averaging of the tower data are taken into account and use of the 2nd moments of the radar Doppler spectrum for sounding presently seems questionable.

8. Height profiles of turbulence parameters

Height profiles of ϵ and C_T^2 are shown in Figs. 16 and 17 for 1812 MST when the inversion layer was in the midtower height range. Fig. 16 shows more than an order-of-magnitude decrease in ϵ in the lowest 50 m. It then increases in the lower part of the stable

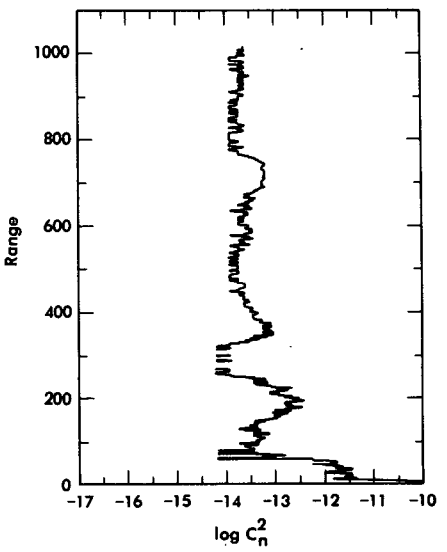

FIG. 14. Height profile of radar-measured C_n^2.

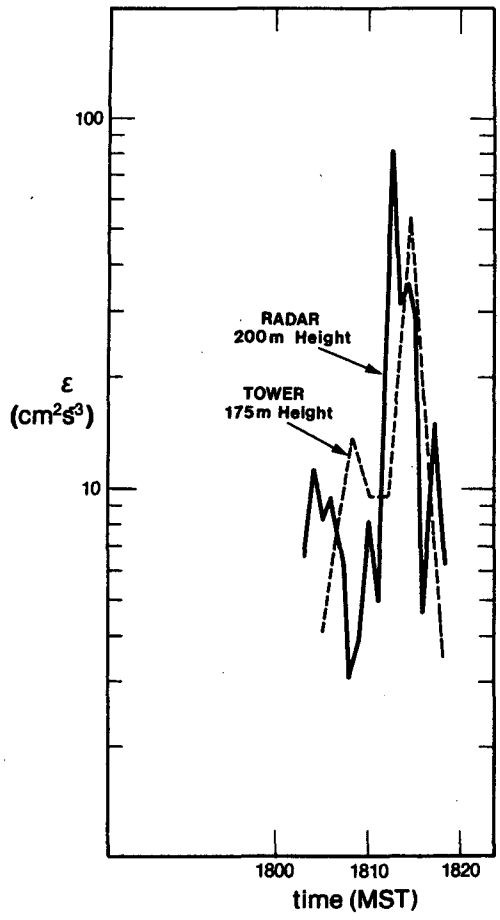

FIG. 15. Tower-measured versus radar-measured turbulent dissipation rate at times shown.

layer but falls to very low values in the upper part and above the inversion. From (18) the Kolmogoroff microscale, η, can be calculated, and the inner scale of turbulence found. The scale of importance in Bragg backscatter is $\lambda/2$ where λ is the radar wavelength. Therefore the critical radar wavelength, λ_c, at which the backscattered power is significantly reduced by viscosity can be calculated from η. We have chosen the

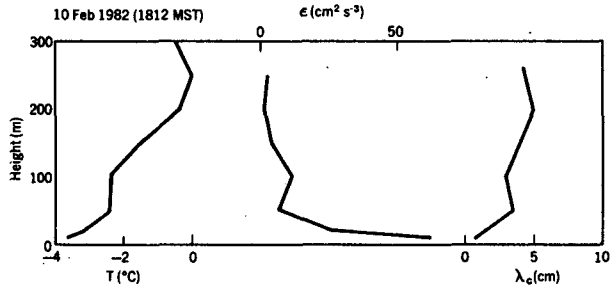

FIG. 16. Height profiles of ϵ and λ_c (cutoff radar wavelength) throughout the thermally stable layer studied in this paper.

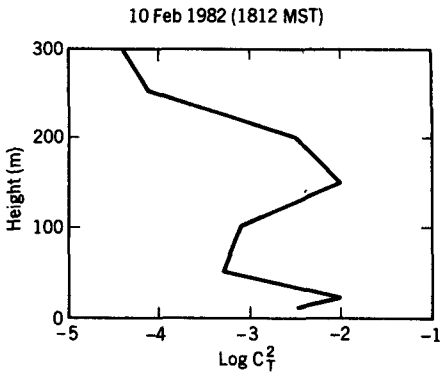

FIG. 17. Height profile of C_T^2 at 1812 MST deduced from temperature spectra found from time series recorded at fixed levels on the tower.

wavelength corresponding to the scale at which the spectral power is reduced by viscous effects to one-half that of the inertial subrange. Thus we have used $\lambda_c = 8\pi\eta$ where the constant 8π is found by choosing the value of k at the point shown in Fig. 18 taken from Fig. 6 of Hill (1978). Fig. 16 shows that the critical wavelength exceeds that of X band radars ($\sim$3 cm) at midtower heights and suggests that even for tropospheric radar returns the wavelength of clear-air radars should be much longer than 5 cm to ensure that they will never encounter severe loss of backscatter, due to viscosity under conditions of weak turbulence.

9. Conclusions

1) Under conditions of thermal stability, the coherence (and correlation) between turbulent fluctuations of temperature and humidity is very high (essentially unity). Therefore the cross-spectrum of temperature and humidity makes an important contribution to the refractive index spectrum as proposed by Gossard (1960). For typical inversion conditions of positive temperature gradient and negative

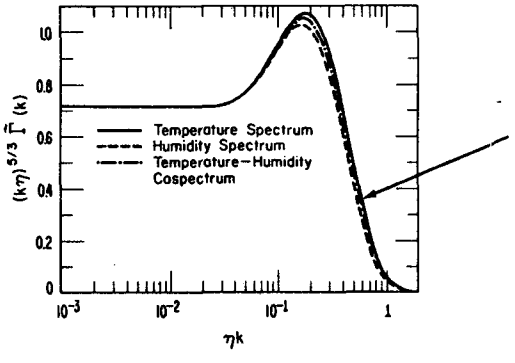

FIG. 18. Theoretical temperature and humidity spectra and temperature–humidity cospectrum. Symbols defined in Hill (1978).

humidity gradient, it increases the power in the refractive index spectrum by a factor of about two.

2) Over a fairly wide range of Richardson number and turbulent dissipation rate, the ratio of the length scales (see Eq. (4)) for temperature, humidity and refractive index to velocity were approximately unity and showed no clear dependence on Ri or ϵ.

3) The values of C_n^2 calculated from the clear-air radar return agreed very well with *in situ* measurements using a platinum wire thermometer and a Lyman-α humidiometer.

4) The values of ϵ calculated from the width of radar-measured Doppler spectrum sometimes showed fairly satisfactory agreement with the *in situ* measured values, but often the agreement is poor. This experiment was not able to verify the accuracy of radar measurements of ϵ.

5) Turbulent dissipation rate fell off drastically through the surface layer, which in this case was capped by a low elevated inversion, and λ_c increased so greatly in the region in and above the inversion that short wavelength radars would have suffered reduced signals because of viscous damping of the crucial turbulence scales.

REFERENCES

Frisch, A. S., and S. F. Clifford, 1974: A study of convection capped by a stable layer using Doppler radar and acoustic echo sounders. *J. Atmos. Sci.*, **31**, 1622–1628.

Gossard, E. E., 1960: Power spectra of temperature, humidity, and refractive index from aircraft and tethered balloon measurements. *IRE Trans. Antennas Propag.*, **AP-8**,186–201.

——, and R. G. Strauch, 1983: *Radar Observation of Clear Air and Clouds.* Elsevier, 280 pp.

——, R. B. Chadwick, W. D. Neff and K. P. Moran, 1982: The use of ground-based Doppler radars to measure gradients, fluxes and structure parameters in elevated layers. *J. Appl. Meteor.*, **21**, 211–226.

Hill, R. J., 1978: Spectra of fluctuations in refractivity, temperature, humidity, and the temperature–humidity cospectrum in the inertial and dissipation ranges. *Radio Sci.*, **13**, 953–961.

Kaimal, J. C., and J. E. Gaynor, 1983: The Boulder Atmospheric Observatory. *J. Climate Appl. Meteorol.*, **22**, 863–880.

Labitt, M., 1981: Coordinated radar and aircraft observations of turbulence. Project Report ATC-108, MIT Lincoln Laboratory, 40 pp.

Tatarskii, V. I., 1971: The effects of the turbulent atmosphere on wave propagation. U.S. Dept. Commerce, 472 pp. [NTIS TT-68-50464].

Wyngaard, J. C., W. T. Pennell, D. H. Lenshow and M. A. LeMone, 1978: The temperature–humidity covariance budget in the convective boundary layer. *J. Atmos. Sci.*, **35**, 45–58.